Available online at www.sciencedirect.com

SciVerse ScienceDirect

Ceramics International 39 (2013) 4017–4030

CERAMICS INTERNATIONAL

www.elsevier.com/locate/ceramint

Water migration in clay slabs during drying: A three-dimensional numerical approach

Wilton Pereira da Silva*, Laerson Duarte da Silva, Vera Solange de Oliveira Farias, Cleide Maria Diniz Pereira da Silva e Silva

Federal University of Campina Grande, Paraiba, Brazil

Received 27 September 2012; received in revised form 24 October 2012; accepted 26 October 2012
Available online 3 November 2012

Abstract

Clay products for construction offer durability, thermal and acoustic comfort as well as low cost. Drying is an important stage of the production process of these products, and it was studied herein. Experiments on convective drying of clay slabs with initial moisture content of 0.23 (db) were performed at 50, 60, 70, 80 and 90 °C. Drying occurred in two distinct periods: constant and falling rate. In the first period, the process was described by an empirical equation and, in the second one, by the diffusion equation with boundary condition of the third kind. To eliminate some restrictions found in the literature, a three-dimensional numerical approach was used to describe the process. Equations were obtained to express the process parameters as a function of the drying air temperature and local moisture content. A simulation using the values obtained from these equations for the process parameters is coherent with the experimental data.
© 2012 Elsevier Ltd and Techna Group S.r.l. All rights reserved.

Keywords: Effective mass diffusivity; Numerical simulation; Optimization; Parallelepiped

1. Introduction

The products manufactured by the ceramic industry for construction and other purposes usually offer durability, thermal and acoustic comfort and low cost. In this industry, drying is an important stage of the production process and contributes significantly to the quality of the final product. According to Silva et al. [1] and several other authors, during drying internal stresses occur due to the gradients of temperature and moisture, and these stresses can produce defects [2–5] or the loss of the product [6,7]. Due to this fact, drying processes of clay materials constitute a subject of great interest in the literature [1–16]. In order to describe water migration within a product, several models are available in the literature and, particularly for ceramic materials, the following can be cited: empirical models [9,12]; semi-empirical models [12]; models based on Darcy law [10,14,16] and diffusion models [1,11–13,15]. Among these models, the simplest is the empirical one, which requires only a linear or nonlinear regression to describe drying kinetics using experimental data. However, these models do not allow determining the moisture distribution within the product, and this distribution is very important in the study of internal strain or crack formation. To determine the water distribution, sometimes diffusion models are used to describe a drying process [1,8,13,15], and some of these models will be highlighted in the following.

Collard et al. [8] studied deformations of a clay plate induced by drying. In order to describe the drying process, Collard et al. [8] used a diffusion model with boundary condition of the third kind, assuming the process parameters with constant value. Thus, the analytical solution of the diffusion equation for the infinite slab was used to describe drying. The process parameters were determined using the first term of the series, and the water content

*Corresponding author. Tel.: +55 83 33332962.
E-mail addresses: wiltonps@uol.com.br (W.P. da Silva), laerson.duarte@gmail.com (L.D. da Silva), vera-solange@uol.com.br (V.S. de Oliveira Farias), cleidedps@uol.com.br (C.M.D.P. da Silva e Silva).

0272-8842/$ - see front matter © 2012 Elsevier Ltd and Techna Group S.r.l. All rights reserved.
http://dx.doi.org/10.1016/j.ceramint.2012.10.252

Nomenclature

A,B,C,a,b	coefficients of the discretized diffusion equation (dimensionless) or fitting parameters
D	effective mass diffusivity ($m^2\,s^{-1}$)
E_a	activation energy ($J\,mol^{-1}$)
h	convective mass transfer coefficient ($m\,s^{-1}$)
M	local moisture content at the instant t (db, kg kg^{-1})
$\overline{M}$	average moisture content at instant t (db, kg kg^{-1})
M_0	initial moisture content (db, kg kg^{-1})
M_{∞}	equilibrium moisture content (db, kg kg^{-1})
$\overline{M}_i^{exp}$	measured value of the moisture content for the experimental point i (db, kg kg^{-1})
$\overline{M}_i^{sim}$	simulated moisture content for the experimental point i (db, kg kg^{-1})
M_P^0	moisture content in the control volume P at the beginning of a time step (db, kg kg^{-1})
N_p	number of experimental points (dimensionless)
N_i, N_j, N_k	number of control volumes in the axes x, y and z
R^2	coefficient of determination (dimensionless)
t	drying time (s)
T	temperature (°C)
V	volume of the parallelepiped (m^3)
x, y, z	Cartesian coordinates (m)
ΔV	volume of a control volume (m^3)
φ''	water flux in the interfaces of a control volume (kg kg^{-1} s^{-1})
σ_i	standard deviation of the experimental point i (db, kg kg^{-1})
χ^2	chi-square or objective function (dimensionless)

profiles were programmed on a computer with a series of 10 terms. According to the authors, the proposed model well describes the drying process. In another work, Chemkhi and Zagrouba [13] determined the water diffusion coefficient of clay material with dimensions $15.0 \times 12.0 \times 1.5\,cm^3$ from drying data. To this end, the authors used a diffusion model, assuming the boundary condition of the first kind to describe the process. An analytical solution was used to describe the whole process, and the series that represents such solution was reduced to the first term. The authors used a polynomial of second order to express the effective mass diffusivity as a function of the average moisture content. According to the authors, the relation used for the diffusivity well describes the behavior of the process. A third article to be highlighted herein is the study of Silva et al. [1]. These authors described the drying process of roof tiles, shaped from red clay, using a diffusion model. In their study, the researchers used the first 25 terms of the series that represents the analytical solution of the diffusion equation with boundary condition of the first and third kind. To determine the process parameters, the authors coupled the analytical solution to an optimizer based on the inverse method. They concluded that the boundary condition of the third kind is better than the first kind in the description of roof tiles drying. On the other hand, the researchers pointed out the limitations of the model, which uses constant process parameters, and suggested a numerical solution for a more rigorous study.

During the bibliographic research on the description of drying of clay materials using a diffusion model, four main simplifications are observed in several works of the literature, including some articles above-mentioned: (1) consideration of the process parameters with constant value; (2) boundary condition of the first kind; (3) use of the diffusion equation to describe the whole process, including the constant drying rate period; and (4) one-dimensional representation of the geometry of the product. However, it is visually observable in a plot of the experimental data of the drying kinetics that a constant rate period exists and it is significant for, at least, a short time interval at the initial instants (see, for instance, Ref. [8,12,16] or Fig. 5 in this article). It is also observable that the boundary of the first kind does not describe the process in a rigorous way, since some resistance to the water flux on surface of the product always is present in this type of material. Finally, according to Silva et al. [17], during the water migration the internal structure of a product is continuously changing and, consequently, the effective mass diffusivity should be supposed variable. In this sense, it seems appropriate to describe drying of clay materials eliminating the simplifications above-mentioned and, in this case, a numerical solution of the diffusion equation is required. Thus, the objective of this article is defined in the following.

The main objective of this article is to describe water migration in clay slabs during drying, emphasizing two distinct periods. To this end, an empirical and a diffusion model were used to describe the whole process, divided into two periods. For the diffusion model, some restrictions such as constant process parameters and representation one-dimensional of the geometry (among others) were eliminated and, due to this fact, a three-dimensional numerical solution was proposed to study the problem in the falling rate period.

2. Material and methods

2.1. Discretization of the diffusion equation in Cartesian coordinates

In a general way, the diffusion equation used to describe a drying process is written as [18–20]:

$$\frac{\partial M}{\partial t} = \nabla(D\nabla M) \tag{1}$$

In Eq. (1), M is the moisture content in dry basis (db), t is the time, and D is the effective mass diffusivity. In Cartesian coordinates, Eq. (1) is written as:

$$\frac{\partial M}{\partial t}=\frac{\partial}{\partial x}\left(D\frac{\partial M}{\partial x}\right)+\frac{\partial}{\partial y}\left(D\frac{\partial M}{\partial y}\right)+\frac{\partial}{\partial z}\left(D\frac{\partial M}{\partial z}\right) \tag{2}$$

where x, y and z are Cartesian coordinates of position.

In this article, Eq. (2) is numerically solved for a parallelepiped-shaped body, assuming the following assumptions: (1) liquid diffusion is the only mechanism that occurs in the falling drying rate period; (2) the effective mass diffusivity D can vary during the diffusion process, while the convective mass transfer coefficient h is considered constant; (3) the parallelepiped is considered homogeneous and isotropic; and (4) in the falling drying rate period, the drying process occurs at isothermal conditions.

The numerical solution was performed using the finite volume method, with a fully implicit formulation [17,21,22] and, consequently, the domain was divided into control volumes. In the three-dimensional case, the domain should be divided into 27 types of control volumes, as shown in Fig. 1.

Observing Fig. 1 it is possible to distinguish 8 control volumes with three faces in contact with the external medium, 12 types of control volumes with 2 faces in contact with the ambient, while 6 types of control volumes have only one of the faces in contact with the external medium. To complete, there are also the internal volumes, with no contact with the external medium.

2.1.1. Internal control volumes

Integrating Eq. (2) on space ($\Delta x\Delta y\Delta z$) and time (Δt), the following expression is obtained:

$$\begin{aligned}\left(M_P-M_P^0\right)\Delta x\Delta y\Delta z &= D_e\frac{M_E-M_P}{\Delta x_e}\Delta z\Delta y\Delta t\\ &\quad -D_w\frac{M_P-M_W}{\Delta x_w}\Delta z\Delta y\Delta t\\ &\quad +D_n\frac{M_N-M_P}{\Delta y_n}\Delta z\Delta x\Delta t-D_s\frac{M_P-M_S}{\Delta y_s}\Delta z\Delta x\Delta t\\ &\quad +D_f\frac{M_F-M_P}{\Delta z_f}\Delta y\Delta x\Delta t-D_b\frac{M_P-M_B}{\Delta z_b}\Delta y\Delta x\Delta t\end{aligned} \tag{3}$$

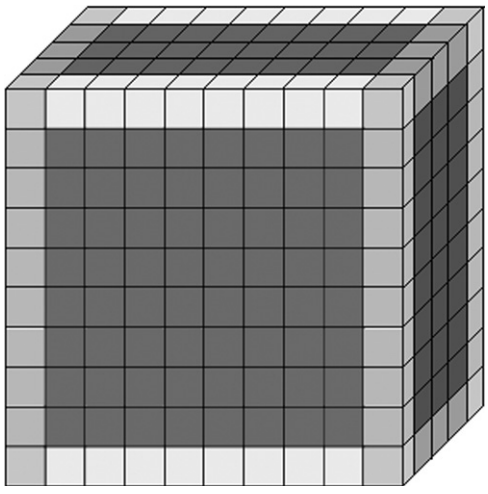

Fig. 1. Types of control volumes in a three-dimensional domain.

Eq. (3) can be organized and written as follows:

$$A_pM_P=A_wM_W+A_eM_E+A_sM_S+A_nM_N+A_bM_B+A_fM_F+B, \tag{4}$$

in which the subscripts "p", "w", "e", "s", "n", "b", and "f" represent, respectively, the nodal point P, west, east, south, north, back and front, as can be observed in Fig. 2.

The coefficients A_p, A_w, A_e, A_s, A_n, A_b, A_f and B of Eq. (4) are given by:

$$\begin{aligned}A_p &= \frac{\Delta x\Delta y\Delta z}{\Delta t}+\frac{D_e}{\Delta x_e}\Delta y\Delta z+\frac{D_w}{\Delta x_w}\Delta y\Delta z\\ &\quad +\frac{D_n}{\Delta y_n}\Delta x\Delta z+\frac{D_s}{\Delta y_s}\Delta x\Delta z\\ &\quad +\frac{D_b}{\Delta z_b}\Delta y\Delta x+\frac{D_f}{\Delta z_f}\Delta y\Delta x\end{aligned} \tag{5a–h}$$

$$A_w=\frac{D_w}{\Delta x_w}\Delta y\Delta z,\ A_e=\frac{D_e}{\Delta x_e}\Delta y\Delta z,\ A_s=\frac{D_s}{\Delta y_s}\Delta x\Delta z,$$
$$A_n=\frac{D_n}{\Delta y_n}\Delta x\Delta z$$
$$A_b=\frac{D_b}{\Delta z_b}\Delta y\Delta x,\ A_f=\frac{D_f}{\Delta z_f}\Delta y\Delta x,\ B=\frac{\Delta x\Delta y\Delta z}{\Delta t}M_P^0$$

In Eq. (5h), M_P^0 is the moisture content in the control volume P at beginning of a time interval Δt.

2.1.2. East control volumes

The control volume to be presented in this topic is in contact with the external medium through the east boundary, as can be seen in Fig. 3. In this figure, the symbols denoted by $M_{\infty e}$ and h_e represent, respectively, the equilibrium moisture content and the convective mass transfer coefficient at the east boundary. The integration of Eq. (2) on space and time for a control volume located at the east boundary results in:

$$A_PM_P=A_WM_W+A_sM_S+A_nM_N+\mathrm{A}_b\mathrm{M}_B+A_FM_F+B \tag{6}$$

and the coefficients A_w, A_s, A_n, A_b and A_f are given by the same expressions provided in Eq. (5). On the other hand, the coefficients A_p and B of Eq. (6) are given by:

$$\begin{aligned}A_p &= \frac{\Delta x\Delta y\Delta z}{\Delta t}+\frac{D_W}{\Delta x_w}\Delta y\Delta z+\frac{D_n}{\Delta y_n}\Delta x\Delta z\\ &\quad +\frac{D_s}{\Delta y_s}\Delta x\Delta z+\frac{D_b}{\Delta z_b}\Delta y\Delta x\\ &\quad +\frac{D_f}{\Delta z_f}\Delta y\Delta x+\frac{\Delta y\Delta z}{\left(\Delta x_e/2D_e\right)+\left(1/h_e\right)}\\ B &= \frac{\Delta x\Delta y\Delta z}{\Delta t}M_P^0+\frac{M_{\infty e}}{\frac{\Delta x_e}{2D_e}+\frac{1}{h_e}}\Delta y\Delta z\end{aligned} \tag{7a, b}$$

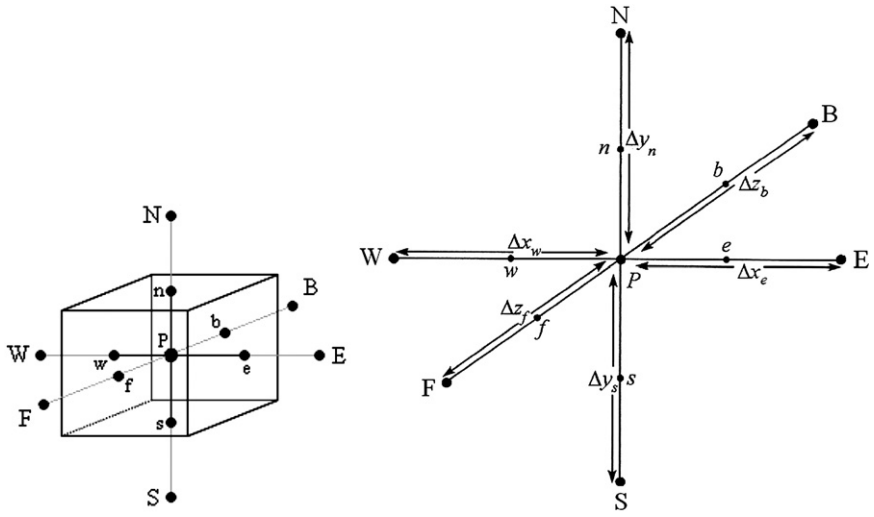

Fig. 2. Internal control volume with nodal point P and its neighbors.

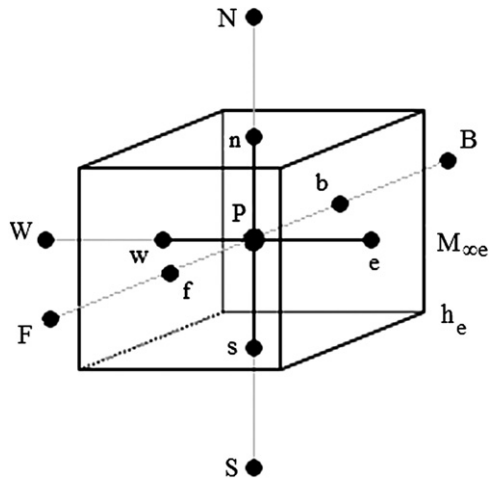

Fig. 3. Control volume located at the east boundary.

Using the same idea to integrate the diffusion equation for the other twenty five types of control volumes, a system of equations for each time step is obtained, and this system can be solved, for instance, by the Gauss–Seidel method.

2.2. Average moisture content

The average value of M can be determined in the following way:

$$\overline{M} = \frac{1}{V}\sum_{i=1}^{N_i}\sum_{j=1}^{N_j}\sum_{k=1}^{N_k} M_{ijk}\Delta V'_{ijk} \tag{8}$$

where

$$V = \sum_{i=1}^{N_i}\sum_{j=1}^{N_j}\sum_{k=1}^{N_k} \Delta V'_{ijk} \tag{9}$$

in which V is the volume of solid; i, j and k define the position of the nodal point of the control volume; M_{ijk} and $\Delta V'_{ijk}$ are, respectively, the moisture content and the volume of the control volume ijk; N_i, N_j and N_k define the number of control volumes in the axes x, y and z, respectively. For a uniform grid, the following relationships must be imposed: $\Delta x_w = \Delta x_e = \Delta x$, $\Delta y_s = \Delta y_n = \Delta y$ and $\Delta z_b = \Delta z_f = \Delta z$. In this case, the volume of a control volume ijk is given by:

$$\Delta V'_{ijk} = \Delta x \Delta y \Delta z \tag{10}$$

and, obviously, $\Delta V'_{ijk}$ is independent of i, j and k for a uniform grid.

2.3. Effective mass diffusivity at interfaces of the control volumes

The effective mass diffusivity in a nodal point is calculated using an appropriate relation between such parameter and the local moisture content M,

$$D = f(M, a, b), \tag{11}$$

where "a" and "b" are parameters that fit the numerical solution to the experimental data, and they are determined by optimization.

On the interfaces of the control volumes, for example "e", assuming a uniform grid, the following expression should be used to determine D [21,23]:

$$D_e = \frac{2D_P D_E}{D_P + D_E}. \tag{12}$$

It is interesting to observe that a subscript in lowercase refers to an interface while a subscript in uppercase refers to a nodal point. On the other hand, as can be seen in Eqs. (5a–h) and (7a,b), Eq. (12) and similar ones are required because the diffusivities that appear in the coefficients "A" must be given at the interfaces of the control volumes.

In this paper, the effective mass diffusivity D is related with the local moisture content M through Eq. (13):

$$D = a + bM, \tag{13}$$

in which a and b are parameters to be determined by optimization, using the obtained experimental dataset. Thus, to describe the process by diffusion for each drying air temperature, three parameters must be determined by optimization: a, b, and the convective mass transfer coefficient h, considered constant for a given temperature of the drying air.

2.4. Process parameters and temperature of the drying air

In this article, the simultaneous dependence of the effective mass diffusivity D on both drying air temperature T and local moisture content M is given by [24,25]:

$$D = (A_1 M + B_1)\exp[-C_1/(T + 273.15)], \tag{14}$$

where A_1, B_1 and C_1 are fitting parameters to be determined by nonlinear regression. Eq. (14) describes the simultaneous dependence of the diffusivity D on M and T, and a comparison of this equation with an Arrhenius type equation

$$D = D_0 \exp\left(-\frac{E_a}{R(T + 273.15)}\right) \tag{15}$$

reveals that E_a/R is equivalent to the parameter C_1, and D_0 is a coefficient equivalent to the factor $(A_1 M + B_1)$. In Eq. (15), E_a is the activation energy (J mol^{-1}) and R is the universal gas constant (8.314 J mol^{-1} K^{-1}).

Supposing that the convective mass transfer coefficient is constant for a given temperature of the drying air, an equation Arrhenius type can be proposed to relate h and T:

$$h = A_2 \exp\left[-\frac{B_2}{(T + 273,15)}\right], \tag{16}$$

where A_2 and B_2 are fitting parameters.

For the constant drying rate period, an expression for $d\overline{M}/dt$ as a function of the drying air temperature can be obtained using nonlinear regression, as it will be seen in this article.

2.5. Optimization

For the falling rate period, the drying process will be described by the diffusion equation. In this case, the process parameters are determined by optimization. The algorithm to be used was presented by Silva et al. [17] and also by Da Silva and Silva [23], and will be reviewed here. In order to determine the parameters D and h by optimization, for a given temperature of the drying air, the objective function was defined by the chi-square referring to the fit of the simulated curve to the experimental data of the drying kinetics. The expression for the chi-square is given by [26,27]

$$\chi^2 = \sum_{i=1}^{N_p} [\overline{M}_i^{\exp} - \overline{M}_i^{sim}]^2 \frac{1}{\sigma_i^2}, \tag{17}$$

where $M_i^{\exp}$ is the average moisture content measured in the experimental point "i" (db), M_i^{sim} is the correspondent simulated moisture content (db), N_p is the number of experimental points, $1/\sigma_i^2$ is the statistical weight referring to the point "i". If the statistical weights are unknown, they can be made equal to a common value, for instance 1. In Eq. (17), the chi-square depends on M_i^{sim}, which depends on D and h. If the convective mass transfer coefficient can be considered constant during a drying process and the effective mass diffusivity is given by Eq. (13), the involved parameters can be determined through the minimization of the objective function, which is accomplished in cycles involving the following steps [17,23]:

Step (1) inform the initial values for the parameters "a", "b" and "h". Solve the diffusion equation and determine the chi-square.
Step (2) inform the value for the correction of "h".
Step (3) correct the parameter "h", maintaining the parameter "a" and "b" with constant values. Solve the diffusion equation and calculate the chi-square.
Step (4) compare the latest calculated value of the chi-square with the previous one. If the latest value is smaller, return to the step 2; otherwise, decrease the last correction of the value of "h" and proceed to step 5.
Step (5) inform the value for the correction of "a".
Step (6) correct the parameter "a", maintaining the parameters "b" and "h" with constant values. Solve the diffusion equation and calculate the chi-square.
Step (7) compare the latest calculated value of the chi-square with the previous one. If the latest value is smaller, return to the step 5; otherwise, decrease the last correction of the value of "a" and proceed to step 8.
Step (8) inform the value for the correction of "b".
Step (9) correct the parameter "b", maintaining the parameters "a" and "h" with constant values. Solve the diffusion equation and calculate the chi-square.
Step (10) compare the latest calculated value of the chi-square with the previous one. If the latest value is smaller, return to the step 8; otherwise, decrease the last correction of the value of "b" and proceed to step 11.
Step (11) begin a new cycle coming back to the step 2 until the stipulated convergence for the parameters "a", "b" and "h" is reached.

According to Da Silva and Silva [23], in each cycle the value of the correction of each parameter can be initially modest, compatible with the tolerance of convergence imposed to the problem. For a given cycle, in each return to the step 2, 5 or 8, the value of the new correction can be multiplied by the factor 2. If the modest correction initially

informed does not minimize the objective function, in the next cycle its value can be multiplied by the factor -1.

2.6. General considerations

In order to economize computer memory and processing time, only a symmetrical piece equivalent to 1/8 of the parallelepiped was studied, as shown in Fig. 4.

For the physical situation shown in Fig. 4, a value equal to zero must be imposed to the water fluxes φ'' at the boundaries west, south and back, which means to impose $h_w=h_s=h_b=0$. For the other boundaries (north, east and front), a common value h was considered for the convective mass transfer coefficient: $h_n=h_e=h_f=h$.

The tolerance for the calculation of the moisture content in each control volume, during the iterative solution of the system of equations via Gauss–Seidel, was of 10^{-8}. On the other hand, the relative tolerance for the calculations of the parameters "a" and "b" (effective mass diffusivity), and "h" (convective mass transfer coefficient), to be obtained by optimizations, was of 10^{-4}.

2.7. Experimental datasets

The raw material used in this research was red clay originated from Parelhas that is a city located in the state of Rio Grande do Norte, Brazil. The chemical composition of clay is 41.80% SiO_2; 22.09% Al_2O_3; 10.43% Fe_2O_3; 3.79% MgO; 2.69% K_2O; 1.25% CaO and others. Complete chemical composition of clay and its size distribution is presented by Silva et al. [1]. Initially, the clay was dried at 110 °C, de-agglomerated in a ball mill and sieved through 80-mesh sieve (180 μm). The powder was homogenized with water up to a moisture content of 0.23 (db), and the obtained mass was kept standing for 24 h to improve the plasticity. The clay slabs were obtained by extrusion using a Verdés Extruder Equipment manufactured in Itu, Sao Paulo, Brazil. The mass shaped as slab was cut by hand and, after removal of the defective parts, each piece was individually packaged in a sealed plastic bag and stored until the beginning of the drying process.

Samples in duplicates were placed in a kiln with mechanical circulation of air and digital temperature controller, model 320E, FANEM, manufactured in Sao Paulo, Brazil. The drying processes were accomplished for five different temperatures (50, 60, 70, 80 and 90 °C), and the air velocity, measured with a digital hygrometer ICEL model HT 208, was 0.07 m s^{-1}. The digital hydrometer was also used to measure the temperature (25 °C on average) and the relative humidity (75% on average) of the room in which the kiln was located. Before placing the test bodies in the oven, they were weighed and their dimensions were measured. To measure the dimensions of the slabs, a digital caliper Digimess, model 100.174 L was used. Measurement of the masses was accomplished with a digital scale Marte, model AL 500C. The slabs were weighed and the dimensions were measured at time intervals ranging from 10 min at the beginning of drying, up to about 2.5 h, at the end of the process. The process took place until the mass reached its equilibrium value. At the end of each drying, the oven temperature was set at 105 °C and the test bodies remained there for 24 h. In this time interval, a new equilibrium was reached, enabling the measurement of dry matter. As a result of these procedures, the experimental data about drying can be summarized in Table 1.

In Table 1, the data relative to 50, 60, 70 and 90 °C were used to determine the values of the process parameters for each temperature during drying. With the determined values, equations to determinate such parameters as a function of the air drying temperature were obtained by curve fitting, using LAB Fit Curve Fitting Software (http://www.labfit.net). The data of Table 1 referring to 80 °C were used to test the obtained expressions. In this case,

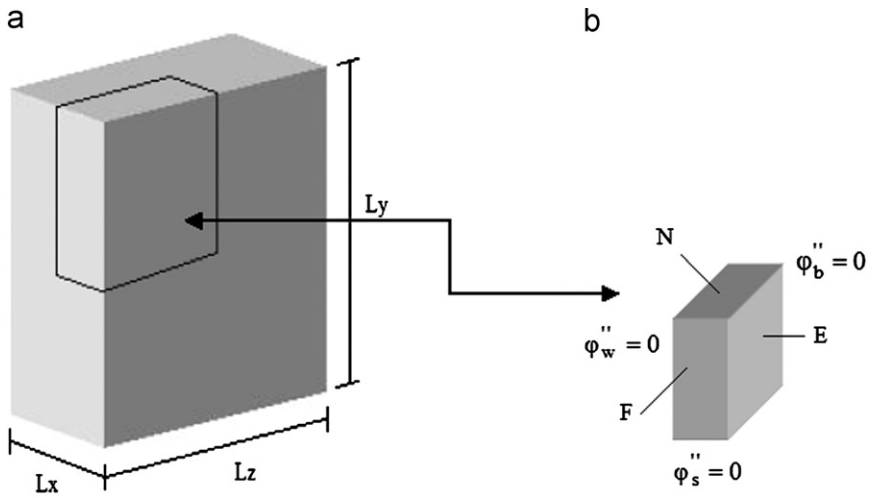

Fig. 4. (a) Parallelepiped highlighting a symmetrical piece; (b) symmetrical piece showing the boundaries with flux equal to zero.

Table 1
Drying air temperature (T), initial moisture content (M_0), equilibrium moisture content (M_{eq}) and dimensions of the clay slabs.

T (°C)	M_0 (db)	M_{eq} (db)	Thickness (m)	Height (m)	Length (m)
50.0	0.2272	0.0162	6.05×10^{-3}	29.38×10^{-3}	77.50×10^{-3}
60.0	0.2286	0.0105	6.02×10^{-3}	24.38×10^{-3}	73.75×10^{-3}
70.0	0.2330	0.0077	5.96×10^{-3}	26.24×10^{-3}	77.13×10^{-3}
80.0	0.2232	0.0048	6.13×10^{-3}	28.70×10^{-3}	81.66×10^{-3}
90.0	0.2316	0.0024	5.92×10^{-3}	26.94×10^{-3}	77.86×10^{-3}

the parameters D and h and the drying rate were calculated through the obtained expressions and these values were used to simulate the drying kinetics, which was compared with the experimental data.

3. Results and discussion

3.1. Experimental results

Experimental datasets referring to the drying kinetics are shown through Fig. 5. A visual inspection in this figure enables to observe that drying occurs in two distinct periods: constant and decreasing rate. An arrow indicates the point where the change of rate occurs. For the five cases, this change occurs near the average moisture content of 0.11 (db).

Based on the experimental results, it was possible to identify two distinct periods of drying rate, and herein the analyses of the drying process were performed separately for each period. In Fig. 5, the limits between the two distinct periods were visually identified at the instants $t = 50$, 36, 29, 22, and 25 for the drying air temperature given respectively by $T = 50$, 60, 70, 80 and 90 °C. On the other hand, Fig. 6 shows the volume of the clay slab as a function of the average moisture content.

As seen from Fig. 6, during the falling drying rate period, the volume is approximately constant, and thus, the dimensional variations can be considered negligible.

3.2. Drying: constant rate period

For the constant drying rate period, the average moisture content as a function of the time can be given by a simple empirical relationship of the first order:

$$\overline{M} = -\frac{d\overline{M}}{dt}t + M_0, \tag{18}$$

and, obviously, Eq. (18) can be obtained by the integration of the relation that defines a constant rate: $-d\overline{M}/dt \equiv c$ being c a constant.

In this case, the optimization process to determine the parameter $-d\overline{M}/dt$ is a simple linear regression. Thus, the obtained results for the drying rates as well as the statistical indicators can be summarized in Table 2.

The drying kinetics at 50, 60, 70 and 90 °C for the constant drying rate period can be observed through Fig. 7.

LAB Fit was developed with a particular characteristic: this software has a library with over 200 functions with one independent variable. If a dataset is provided to the program, each function of its library is automatically fitted to the data, and the best results are classified by comparison of the reduced chi-square referring to each fit. This tool, available in an option called "Finder", was used to determine a function with three parameters to express the rate $-d\overline{M}/dt$ as a function of the drying air temperature, using the data (T, $-d\overline{M}/dt$) given in Table 2. One of the best functions determined by LAB Fit was the Gunary equation:

$$-\frac{d\overline{M}}{dt} = \frac{T}{A_1 + B_1 T + C_1\sqrt{T}}. \tag{19}$$

The result of the fit of Eq. (19) is shown in Fig. 8(a). From the Gunary equation presented in Fig. 8(a), the value $-d\overline{M}/dt = 4.988 \times 10^{-3}\ \mathrm{min}^{-1}$ is obtained for the temperature of 80 °C. In order to test the model proposed for the constant rate period, the values of the drying rate and initial moisture content at 80 °C were used to simulate the drying kinetics at this temperature, and the result is shown in Fig. 8(b).

3.3. Drying: falling rate period

In this study, the instant in which the drying process begins with the decreasing rate period was considered equal to zero. On the other hand, in the numerical solution of the diffusion equation, the obtained results cannot depend on the established time interval for each step. A study on the refinement of this interval indicates that the drying time with falling rate should be divided into 2200 steps. This quantity of steps can guarantee an adequate time refinement to the problem. With relationship to the grid, using a similar study of refinement, the symmetrical piece shown in Fig. 4 was defined with $20 \times 20 \times 20$ (8000 control volumes), and this implies in 64,000 control volumes for the whole slab. As the experimental results indicate that in the falling rate period the dimensional variations can be considered negligible, such variations were not considered in the optimization and simulation processes.

3.3.1. Optimizations and simulations

Performing optimization processes with the datasets for the drying air temperature at 50, 60, 70 and 90 °C, the obtained results are presented in Table 3.

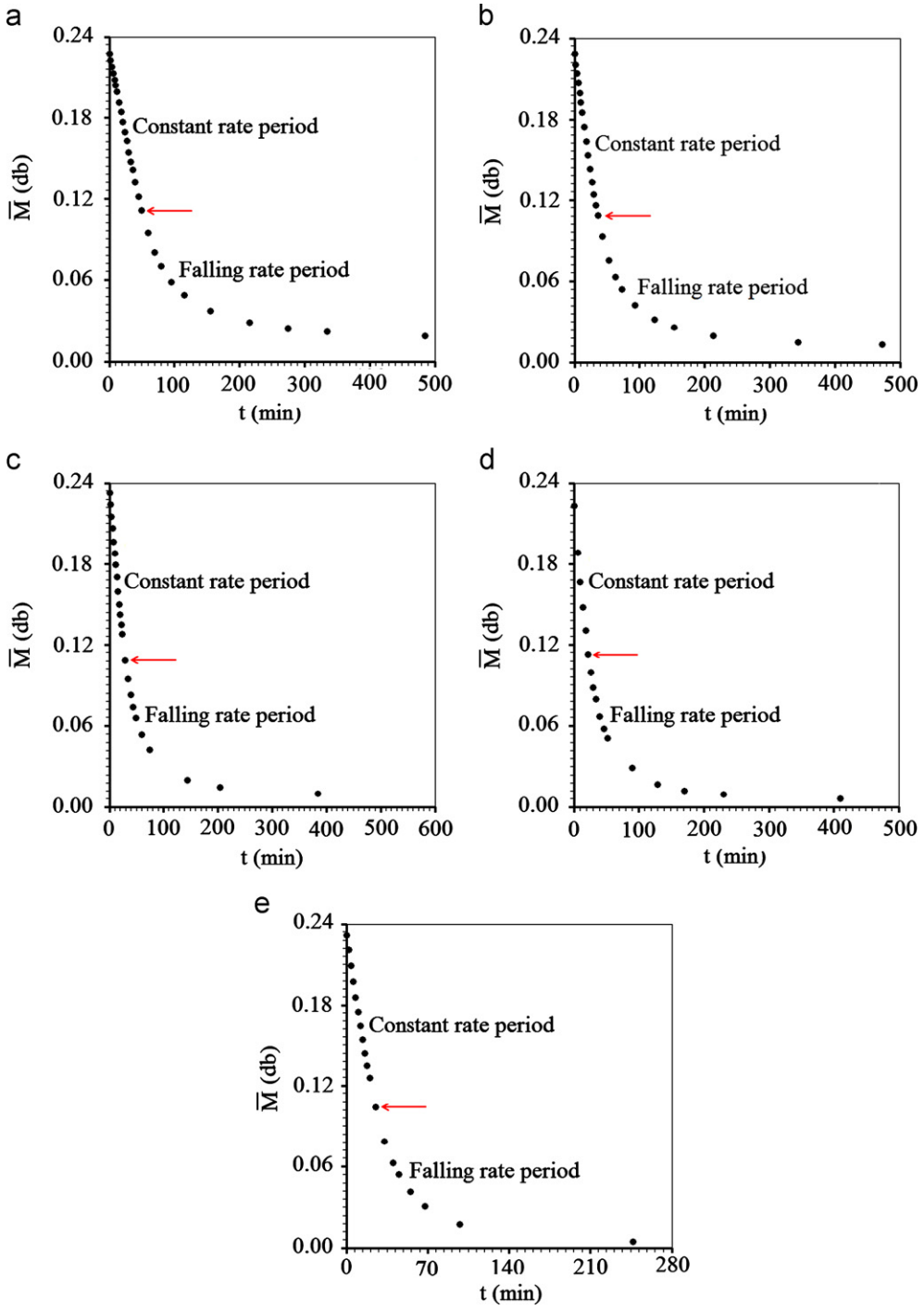

Fig. 5. Experimental datasets of the drying processes at $T=$ (a) 50 °C, (b) 60 °C, (c) 70 °C, (d) 80 °C; (e) 90 °C.

It is interesting to observe that the experimental dataset obtained for the temperature of 80 °C was used only as a test. On the other hand, with the determined process parameters, the simulations of the drying kinetics can be performed and are presented through Fig. 9.

Note that the moisture contents shown in Fig. 9 define the limit of validity for the expressions of the effective mass diffusivity given in Table 3. The superposition of the simulations of the drying processes at temperatures of 50, 60, 70 and 90 °C, from $t=0$ up to $t=440$ min, can be observed in Fig. 10.

3.3.2. *Arrhenius-type equations*

Fig. 11 shows the effective mass diffusivity as a function of the local moisture content for all temperatures for which the process parameters were obtained by optimization.

An inspection in Fig. 11 indicates that the effective mass diffusivity increases with increasing the local moisture content.

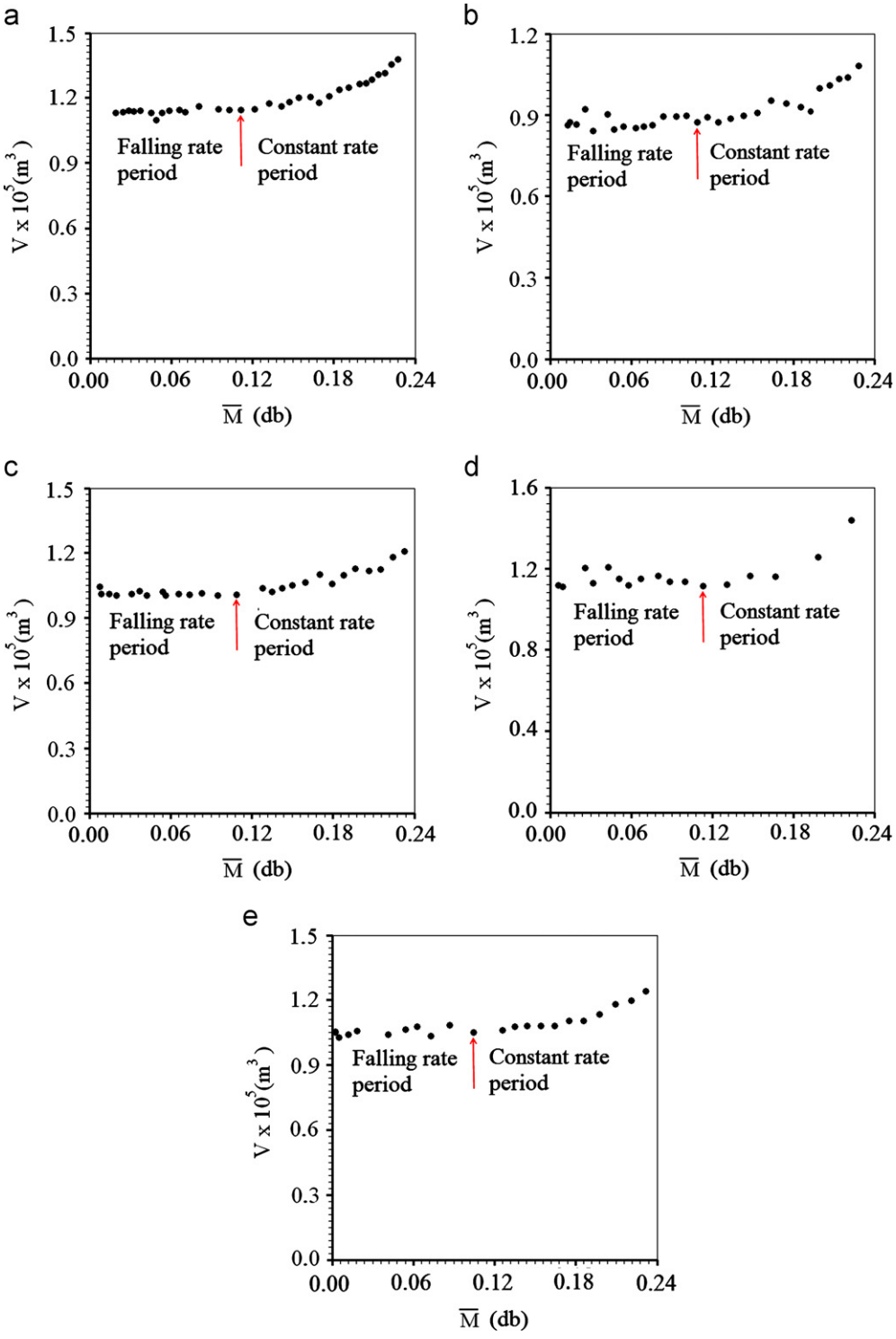

Fig. 6. Graphs of volume of the clay slab as a function of the average moisture content at T=(a) 50 °C; (b) 60 °C; (c) 70 °C; (d) 80 °C; and (d) 90 °C.

Several authors found the same behavior for the water diffusivity in studies of drying [25,28].

The simultaneous dependence of the diffusivity D on both temperature and local moisture content is given by Eq. (14). A new table containing values of D for various local moisture contents can be constructed, for example, M=0.0162, 0.0383, 0.0604, 0.0825 and 0.1046, using the expressions for the effective mass diffusivity given in Table 3 at the temperatures of 50, 60, 70 and 90 °C. By fitting Eq. (14) to this grid of values, the following result is obtained:

$$D = \left(5.042 \times 10^{-3} M - 7.037 \times 10^{-6}\right) \exp\left[-\frac{2581}{(T+273.15)}\right]. \quad (20)$$

Table 2
Results of the fits referring to the drying kinetics during constant rate period.

T (°C)	$-d\overline{M}/dt(\min^{-1})$	R^2	χ^2
50.0	2.367×10^{-3}	0.9992	1.751×10^{-5}
60.0	3.479×10^{-3}	0.9980	6.504×10^{-5}
70.0	4.435×10^{-3}	0.9978	4.655×10^{-5}
90.0	5.344×10^{-3}	0.9964	8.952×10^{-5}

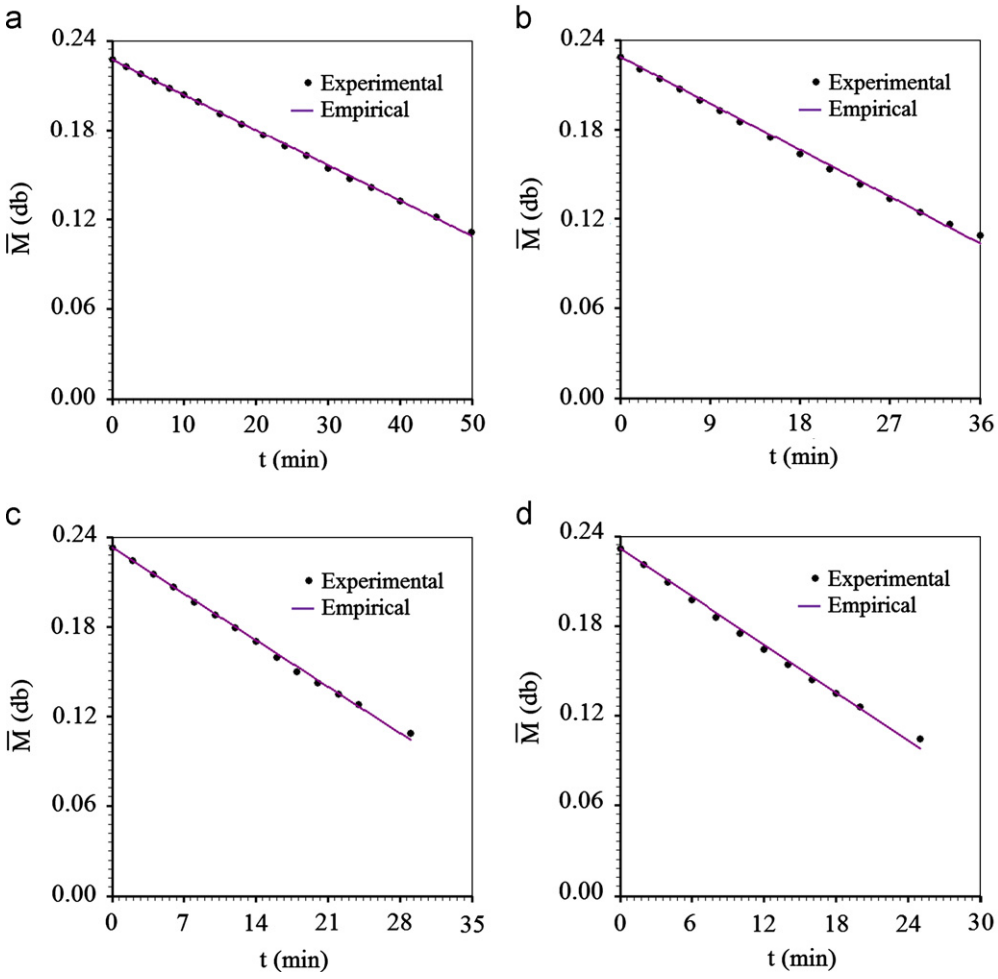

Fig. 7. Drying kinetics for the constant rate period with air at T =: (a) 50 °C; (b) 60 °C°C; (c) 70 °C; and (d) 90 °C.

Thus, using Eq. (20), a graph that shows the simultaneous dependence of the effective mass diffusivity on both, drying air temperature and local moisture content, can be obtained for the following intervals: (1) temperature from 50 to 90 °C, (2) local moisture content from 0.0162 to 0.1046 (db). This graph is shown in Fig. 12.

In the graph of Fig. 12 the full circles are experimental data lying on or above the surface, and the empty circles are below. This graph indicates that the effective mass diffusivity increases not only with the temperature of the drying air but also with the local moisture content.

From the comparison between Eqs. (14) and (15), the activation energy, given by E_a=RC_1 (where $C_1 = 2581$ °C), is obtained: $E_a = 21.46$ kJ mol^{-1}. This value is compatible with values found in the literature for this type of product [1].

Performing the fit of Eq. (16) to the pairs (T,h) available in Table 3, the following result is obtained:

$$h = 8.989 \times 10^{-3} \exp\left[-\frac{1637}{(T+273.15)}\right]. \quad (21)$$

and Eq. (21) is valid for the interval from 50 up to 90 °C.

A graph that shows Eq. (21) for the limit of temperature between 50 and 90 °C is given through Fig. 13.

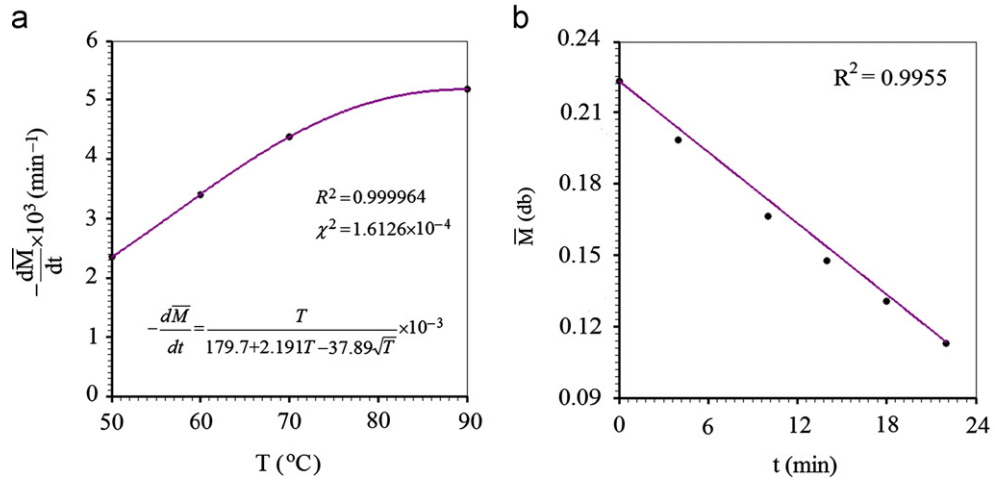

Fig. 8. (a) Drying rate as a function of the air drying temperature obtained by the Gunary equation; (b) Simulation of the drying kinetics for the constant drying rate period with air at T=80 °C.

Table 3
Process parameters obtained by optimization and statistical indicators.

	D(m^2 min^{-1})	$2.242\times10^{-6}M-3.051\times10^{-8}$
50 °C	h (m min^{-1})	5.577×10^{-5}
	χ^2	1.710×10^{-6}
	R^2	0.99984
	D (m^2 min^{-1})	$2.271\times10^{-6}M-1.769\times10^{-8}$
60 °C	h (m min^{-1})	6.439×10^{-5}
	χ^2	1.413×10^{-6}
	R^2	0.99988
	D (m^2 min^{-1})	$2.680\times10^{-6}M-0.690\times10^{-8}$
70 °C	h (m min^{-1})	8.004×10^{-5}
	χ^2	7.667×10^{-7}
	R^2	0.99993
	D (m^2 min^{-1})	$3.902\times10^{-6}M+1.566\times10^{-8}$
90 °C	h (m min^{-1})	9.790×10^{-5}
	χ^2	4.634×10^{-7}
	R^2	0.99994

3.3.3. Drying at 80 °C

In order to test the model proposed for the falling drying rate period, Eqs. (20) and (21) were used to determine D and h at T=80 °C, and this resource dispenses the optimization process which is relatively slow. The following results were obtained: $D=3.365\times10^{-6}M,\ -4.713\times10^{-9}$ m^2 min^{-1} and $h=8.721\times10^{-5}$ m min^{-1}. Thus, performing a simulation of the drying kinetics, the obtained results are presented, together with the experimental data, through Fig. 14.

According to the results, performing the simulation at 80 °C with the parameters determined by Eqs. (20) and (21), the statistical indicators were $R^2=0.99916$ and $\chi^2=1.1639\times10^{-5}$.

3.4. Discussion

It is interesting to observe that the numerical solution developed for the diffusion equation is general, valid for a problem with no symmetry. In this case, it is only necessary to study the whole parallelepiped instead a symmetrical piece.

The experimental results obtained in this article are similar to others found in the literature for convective drying of clay products with initial moisture content greater than 0.11 (db), as can be seen in Refs. [8,12,16]. In these works, it is possible to identify two distinct periods: constant and falling rate. In relationship to the shrinkage, this phenomenon was significant from the initial moisture content up to about 0.11 (db), and similar result was found by Collard et al. [8] and several other authors.

In the literature, there are works which propose only one model to describe the drying kinetics of the whole process for clay materials. Mihoubi and Bellagi [16] described the drying kinetics of clay sample through a complex model that uses the Darcy law, relating the water migration and the fluid pressure gradient. Simple models are also used to describe drying kinetics such as Page model [12]. However, an empirical model does not allow to predict the moisture distribution within the product in a given instant. In the present paper, an empirical model is used to describe only the constant drying rate period, in which a uniform distribution of moisture is observed [12] and, consequently, the moisture distribution does not need to be predicted.

As is known, but it is interesting to observe even so, the constant rate $-d\overline{M}/dt$ increases with increasing of the drying air temperature T, as can be seen in Table 2. Thus, with the results obtained at 50, 60, 70 and 90 °C, it was possible to fit a Gunary equation to the data $(T,-d\overline{M}/dt)$, and the statistical indicators presented in Fig. 8(a) enables to state that this fitting can be considered good. More than that, this equation enabled to calculate the drying rate for the test temperature of 80 °C. This calculation made it possible to simulate the drying kinetics and the result can be considered reasonable when compared with the experimental dataset for this temperature, as shown in Fig. 8(b).

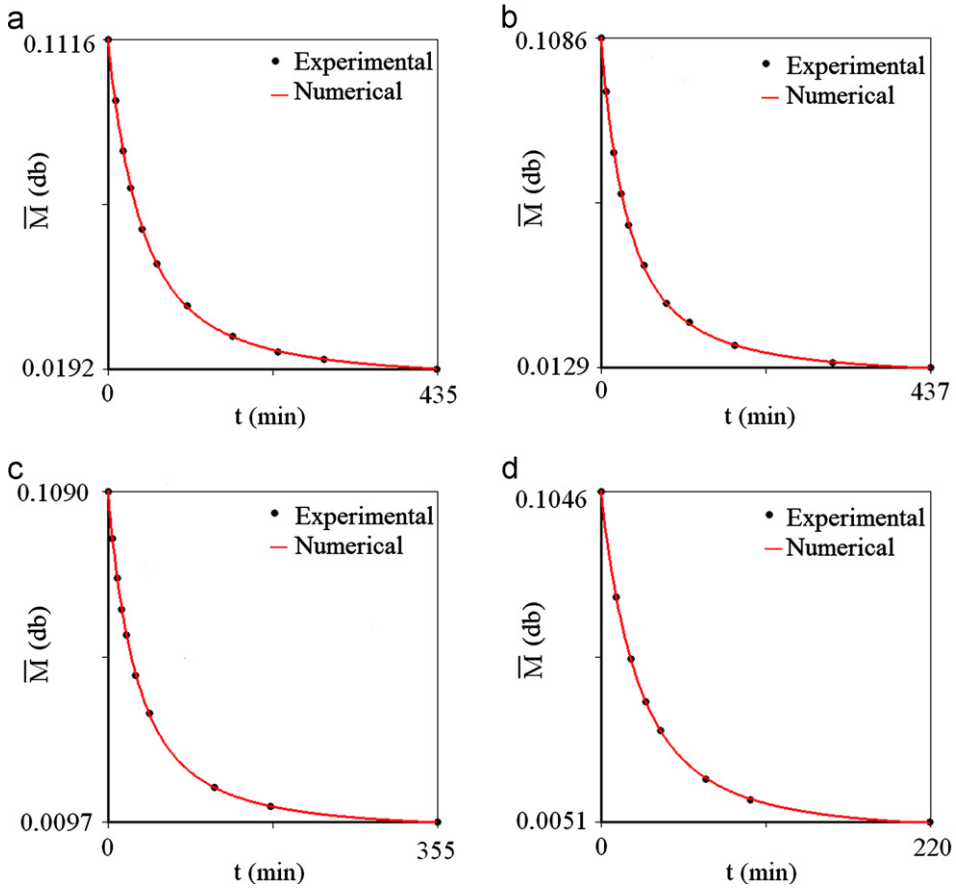

Fig. 9. Simulation of the drying kinetics for the falling rate period with air at T=(a) 50,0 °C; (b) 60 °C; (c) 70 °C; and (d) 90 °C.

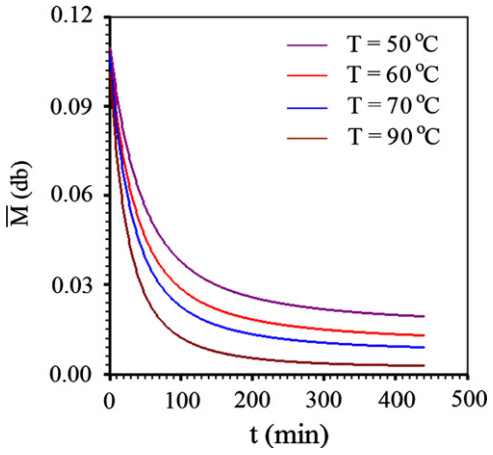

Fig. 10. Superposition of the drying kinetics predicted by the proposed diffusion model.

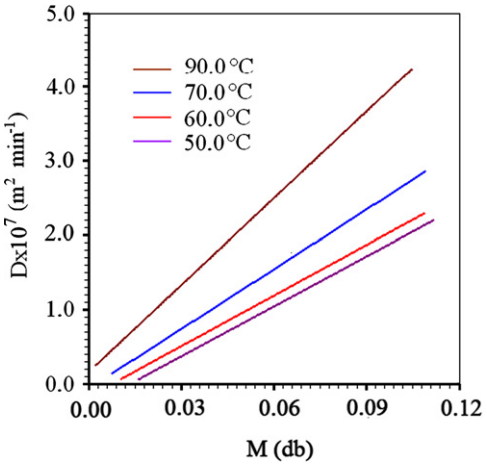

Fig. 11. Effective mass diffusivity of the clay slabs as a function of moisture content at the indicated temperatures.

Some works found in the literature describe the whole drying process in clay products using only the diffusion Eqs. (1,8,12,13). However, the results are not very good, particularly when the effective mass diffusivity is considered constant and the boundary condition is of the first kind, as can be observed in Refs. [1,8]. Thus, in the present article, the diffusion model was used to describe the drying process only in the falling rate period and, even so, the effective mass diffusivity was considered variable, as a function of the local moisture content, and the boundary condition was assumed to be of the third kind. Due to this fact, two particular aspects in the discretization and solution of the diffusion equation deserve to be highlighted. First, as observed by Silva et al. [22], the diffusion

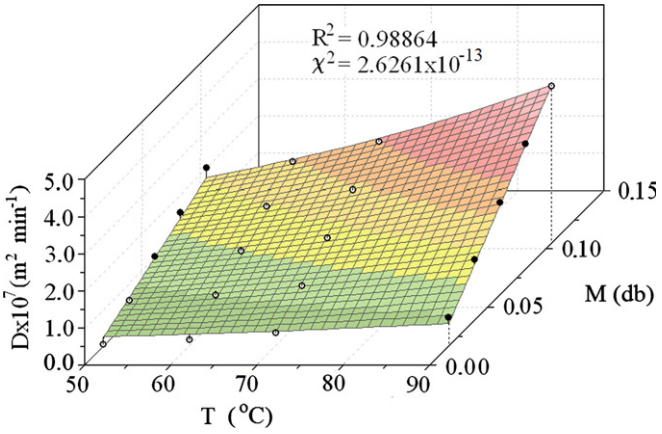

Fig. 12. Graph of the effective mass diffusivity of the clay slabs using Eq. (20).

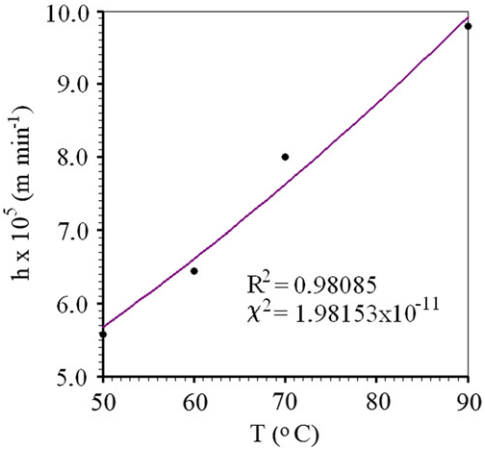

Fig. 13. Convective mass transfer coefficient as a function of the drying air temperature.

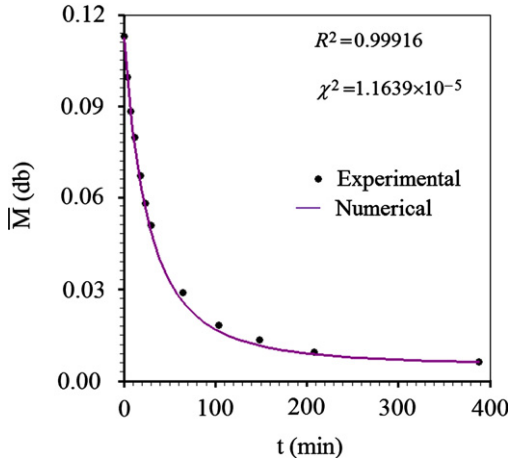

Fig. 14. Simulation of the drying kinetics for the control temperature of 80 °C.

term must be discretized in the form $\nabla(D\nabla M)$ instead $D\nabla^2 M$. This fact enables to consider the effective mass diffusivity with constant or variable value during the process. Second, as the diffusivities at the interfaces of the control volumes can be variable at the time, the coefficients "A" in Eqs. (5) and (7) contain nonlinearities caused by the variations of D during the process. In this case, the coefficients "A" must be recalculated in each time step and the time steps must be small in order to minimize errors due to the nonlinearities. This fact helps to explain the high number of time steps established in this work: 2200. Another aspect to be considered on the diffusion equation solution is the following: although the proposed solution can be used for the case involving dimensional variations, in the present study the shrinkage during the process was not considered. However, the reason is simple: the diffusion model was used to describe only the drying kinetics referring to the falling rate. As it can be observed in Fig. 6, the dimensional variations in this period can be considered negligible. Thus, the dimensions of the slabs used to solve the diffusion equation were those at the beginning of the falling rate period.

In the present paper, a question needs to be answer: what the relevance of the Eqs. (20) and (21) in this study? As is known, an optimization process based on inverse method is relatively slow. Thus, once this process has been used for some temperatures of the drying air, enabling the obtaining of these equations, the optimizations can be substituted by the idea used herein. Eqs. (20) and (21) can be used, instead the optimizations, to describe a drying kinetics at other temperature between 50 and 90 °C. In other words, the parameters D and h can be calculated with no optimization process and then the simulations of the drying kinetics can be performed [1]. In the present article, this resource was used and Figs. 8(b) and 14 were obtained for the constant and falling rate period. In the two cases, the distributions of the experimental points around the simulated lines cannot be considered random. Despite this fact, the statistical indicators of the drying kinetics are very satisfactory.

Finally, despite the present article does not have presented a study about the moisture distribution at a given instant t, during the falling drying rate period, the necessary information for this presentation is generated in each simulation of the proposed numerical solution. Thus, the computational tools developed in this research also serves to study the strain and crack formation during the drying process.

4. Conclusion

Experimental datasets enable to identify two distinct drying periods: constant and falling rate. The transition occurs in an average moisture content of about 0.11 (db) for the five drying air temperatures.

Empirical model well describes the drying kinetics at a constant rate period, and enables to determine the drying rates through a simple linear regression. A Gunary equation made it possible to relate the drying rate with the drying air temperature, and such equation enables to

predict a rate for a drying air temperature specified between 50 and 90 °C. Comparison between drying kinetics predicted at 80 °C (used as test) and experimental data permit to affirm that the obtained Gunary equation enables to predict in a satisfactory way the drying rate for a given temperature of the drying air.

The use of a three-dimensional numerical approach for the diffusion equation enables to avoid some simplifications common in the literature such as the consideration of the process parameters with constant value and the representation one-dimensional of the geometry. Thus, the falling rate period can be described in an accurate way for all drying air temperatures. An Arrhenius-type equation was used with success to relate the effective mass diffusivity with the local moisture content and the drying air temperature. Another Arrhenius-type equation permitted to relate the convective mass transfer coefficient with the drying air temperature. These two equations enable to determine the process parameters, with no need of the optimization, and that make it possible to simulate a drying process between 50 and 90 °C. A simulation at 80 °C enabled to verify that the obtained results are very near of the experimental data for this temperature.

Acknowledgments

We acknowledge partial financial support from the Brazilian organizations Coordenação de Aperfeiçoamento de Pessoal de Nível Superior (CAPES) and the Conselho Nacional de Desenvolvimento Científico e Tecnológico (CNPq).

References

[1] W.P. Silva, V.S.O. Farias, G.A. Neves, A.G.B. Lima, Modeling of water transport in roof tiles by removal of moisture at isothermal conditions, Heat and Mass Transfer 48 (2012) 809–821.
[2] Z.X. Gong, A.S. Mujumdar, Y. Itaya, S. Mori, M. Hasatani, Drying of clay and nonclay media: heat and mass transfer and quality aspects, Drying Technology 16 (1998) 1119–1152.
[3] G. Musielak, Possibility of clay damage during drying, Drying Technology 19 (2001) 1645–1659.
[4] Y. Itaya, S. Uchiyama, S. Hatano, S. Mori, Drying enhancement of clay slab by microwave heating, Drying Technology 23 (2005) 1243–1255.
[5] G. Musielak, D. Mierzwa, Permanent strains in clay-like material during drying, Drying Technology 27 (2009) 894–902.
[6] R. Maciulaitis, J. Malaiškien, A. Kicait, The regulation of physical and mechanical parameters of ceramic bricks depending on the drying regime, Journal of Civil Engineering and Management 14 (2008) 263–268.
[7] R. Maciulaitis, J. Malaiškien, The regulation of structural parameters of ceramics depending on the drying regime, Journal of Civil Engineering and Management 15 (2009) 197–204.
[8] J.M. Collard, G. Arnaud, J.P. Fohr, A. Dragon, The drying-induced deformations of a clay plate, International Journal of Heal Mass Transfer 35 (1992) 1103–1114.
[9] D. Skansi, S. Tomas, Microwave drying kinetics of a clay-plate, Ceramics International 21 (1995) 207–211.
[10] S.L. Su, Modeling of multi-phase moisture transfer and induced stress in drying clay bricks, Applied Clay Science 12 (1997) 189–207.
[11] A.Y. Looi, K. Golonka, M. Rhodes, Drying kinetics of single porous particles in superheated steam under pressure, Chemical Engineering Journal 87 (2002) 329–338.
[12] A. Sander, D. Skansi, N. Bolf, Heat and mass transfer models in convection drying of clay slabs, Ceramics International 29 (2003) 641–653.
[13] S. Chemkhi, F. Zagrouba, Water diffusion coefficient in clay material from drying data, Desalination 185 (2005) 491–498.
[14] S. Chemkhi, F. Zagrouba, Development of a Darcy-flow model applied to simulate the drying of shrinking media, Brazilian Journal of Chemical Engineering 25 (2008) 503–514.
[15] V.S.O. Farias, W.P. Silva, C.M.D.P.S. Silva, A.G.B. Lima, Three-dimensional diffusion in arbitrary domain using generalized coordinates for the boundary condition of the first kind: application in drying, Defect and Diffusion Forum 326–328 (2012) 120–125.
[16] D. Mihoubi, A. Bellagi, Modeling of heat and moisture transfers with stress–strain formation during convective air drying of deformable media, Heat and Mass Transfer 48 (2012) 1697–1705.
[17] W.P. Silva, C.M.D.P.S. Silva, V.S.O. Farias, J.P. Gomes, Diffusion models to describe the drying process of peeled bananas: optimization and simulation, Drying Technology 30 (2012) 164–174.
[18] A.V. Luikov, Analytical Heat Diffusion Theory, Academic Press, Inc. Ltd, London, 1968.
[19] J. Crank, The Mathematics of Diffusion, Clarendon Press, Oxford, UK, 1992.
[20] R.B. Bird, W.E. Stewart, E.N. Lightfoot, Transport phenomena, 2nd Ed., John Wiley & Sons, Inc, New York, 2001.
[21] S.V. Patankar, Numerical Heat Transfer and Fluid Flow, Hemisphere Publishing Corporation, New York, 1980.
[22] W.P. Silva, C.M.D.P.S. Silva, M.A.A. Lins, Determination of expressions for the thermal diffusivity of canned foodstuffs by the inverse method and numerical simulations of heat penetration, International Journal of Food Science and Technology 46 (2011) 811–818.
[23] W.P. Da Silva, C.M.D.P.S. Silva, Calculation of the convective heat transfer coefficient and thermal diffusivity of cucumbers using numerical simulation and the inverse methodJournal of Food Science and Technology, http://dx.doi.org/10.1007/s13197-012-0738-4, in press.
[24] B. Hadrich, N. Boudhrioua, N. Kechaou, Drying of Tunisian sardine (*Sardinella aurita*) experimental study and three-dimensional transfer modeling of drying kinetics, Journal of Food Engineering 84 (2008) 92–100.
[25] W.P. Da Silva, J.W. Precker, A.G.B. De Lima, Drying kinetics of lima bean (*Phaseolus lunatus* L.). Experimental determination and prediction by diffusion models, International Journal of Food Engineering 5 (2009) 1–20.
[26] P.R. Bevington, D,K. Robinson, Data Reduction and Error Analysis for the Physical Sciences, 2nd Ed., WCB/McGraw-Hill, Boston, 1992.
[27] J.R. Taylor, An Introduction to Error Analysis, 2nd Ed., University Science Books, Sausalito, California, 1997.
[28] I.I. Ruiz-López, M.A. García-Alvarado, Analytical solution for food-drying kinetics considering shrinkage and variable diffusivity, Journal of Food Engineering 79 (2007) 208–216.